doi:10.1111/j.1365-2958.2010.07399.x

# Carbon flux rerouting during *Mycobacterium tuberculosis* growth arrest

**Lanbo Shi,[1] Charles D. Sohaskey,[2] Carmen Pfeiffer,[1†] Pratik Datta,[1] Michael Parks,[1] Johnjoe McFadden,[3] Robert J. North[4] and Maria L. Gennaro[1*]**

[1]*Public Health Research Institute, New Jersey Medical School, Newark, NJ 07103, USA.*

[2]*Department of Veterans Affairs Medical Center, Long Beach, CA 90822, USA.*

[3]*Faculty of Health and Medical Sciences, University of Surrey, Guildford, Surrey GU2 5XH, UK.*

[4]*Trudeau Institute, Saranac Lake, NY 12983, USA.*

## Summary

**A hallmark of the *Mycobacterium tuberculosis* life cycle is the pathogen's ability to switch between replicative and non-replicative states in response to host immunity. Transcriptional profiling by qPCR of ~ 50 *M. tuberculosis* genes involved in central and lipid metabolism revealed a re-routing of carbon flow associated with bacterial growth arrest during mouse lung infection. Carbon rerouting was marked by a switch from metabolic pathways generating energy and biosynthetic precursors in growing bacilli to pathways for storage compound synthesis during growth arrest. Results of flux balance analysis using an *in silico* metabolic network were consistent with the transcript abundance data obtained *in vivo*. Similar transcriptional changes were seen *in vitro* when *M. tuberculosis* cultures were treated with bacteriostatic stressors under different nutritional conditions. Thus, altered expression of key metabolic genes reflects growth rate changes rather than changes in substrate availability. A model describing carbon flux rerouting was formulated that (i) provides a coherent interpretation of the adaptation of *M. tuberculosis* metabolism to immunity-induced stress and (ii) identifies features common to mycobacterial dormancy and stress responses of other organisms.**

Accepted 11 September, 2010. *For correspondence. E-mail gennarma@umdnj.edu; Tel. (+1) 973 854 3210; Fax (+1) 973 854 3101. †Present address: Diabetes Discovery Platform, Medical Research Council, Tygerberg, 7505, South Africa.



## Introduction

Tubercle bacilli switch between replicative (growth) and non-replicative (dormancy) states in response to the host environment. Immunity-induced cessation of bacterial growth leads to a chronic, asymptomatic infection that is maintained by persisting tubercle bacilli. When host immunity falters, tubercle bacilli can resume growth and cause disease. Dormant bacilli present a formidable challenge to tuberculosis control, because they are much less susceptible to antibacterial drugs than growing bacilli (Zhang, 2004). Thus, a molecular understanding of events occurring during the transition from growth to dormancy is important for identifying critical targets for new tuberculosis control strategies.

The metabolism of *Mycobacterium tuberculosis* during infection has been an area of intense interest since the origins of tuberculosis research. Seminal experiments showed that the tubercle bacillus, which is metabolically flexible (Wheeler and Ratledge, 1994), preferentially utilizes fatty acids as carbon and energy source during murine infection (Bloch and Segal, 1956). This preferential utilization is likely due to increased availability of lipids in the infected host cell (Russell *et al.*, 2009) and is reflected in the *M. tuberculosis* genome as a significant enrichment for fatty acid degradation genes (Cole *et al.*, 1998). Moreover, genes involved in fatty acid utilization (glyoxylate shunt: *icl*; gluconeogenesis: *glpX* and *pckA*) are required for growth and persistence *in vivo* (Collins *et al.*, 2002; Liu *et al.*, 2003; Sassetti and Rubin, 2003; Munoz-Elias and McKinney, 2005; Marrero *et al.*, 2010). Some of these genes (*icl*, *pckA*) are also upregulated in non-growing bacilli during mouse infection (McKinney *et al.*, 2000; Schnappinger *et al.*, 2003; Timm *et al.*, 2003). These observations led to the proposal that *M. tuberculosis* switches its carbon source from sugars to fatty acids during the persistent phase of infection (Bishai, 2000; Honer zu Bentrup and Russell, 2001; Timm *et al.*, 2003). However, similar metabolic changes are observed in the stress response of other organisms, such as sporulation in yeast (Cortassa *et al.*, 2000), where they are linked to the rerouting of carbon flow towards formation of storage compounds. Indeed, tubercle bacilli obtained from sputum of tuberculosis patients are rich in triacylglycerol (TAG) (Garton *et al.*, 2008), a common storage

compound in Actinobacteria (Alvarez and Steinbuchel, 2002). Therefore, it has been unclear whether the metabolic changes in the tubercle bacillus during infection reflect implementation of a developmental programme towards persistence or an adaptive response to changed nutritional conditions.

In the present work we examined the response of *M. tuberculosis* metabolism to the stress encountered during infection with a multi-scale approach that included studies *in vivo* (mouse infection), *in silico* and *in vitro* (broth culture). We interrogated two aspects of carbon metabolism of tubercle bacilli. One is central metabolism, which provides energy, reducing power and biosynthetic precursors. The other is the biosynthesis of major lipids, such as mycobacterial cell wall components, which constitute a sink for energy and biosynthetic precursors (Brennan, 2003), and triacylglycerol (TAG), which is a storage lipid (Brennan, 2003; Garton *et al*., 2008; Low *et al*., 2009). Transcription profiling of tubercle bacilli during infection of mouse lungs led to a metabolic model in which carbon flow redistributes at the phosphoenolpyruvate (PEP)/pyruvate-oxaloacetate (OAA) node as growth stops, thereby switching from the generation of energy and biosynthetic precursors to the synthesis of storage compounds. The *in vivo* data provided conditions to perform *in silico* simulations of metabolic flux patterns associated with *M. tuberculosis* growth arrest using a genome-scale metabolic network of the tubercle bacillus (Beste *et al*., 2007). We found that metabolic fluxes (i) were largely consistent with the transcription profiles of *M. tuberculosis* central metabolism genes seen during mouse infection and (ii) predicted that utilization of different carbon sources would result in similar flux solutions. This prediction was tested *in vitro* using *M. tuberculosis* cultures subjected to bacteriostatic stress in media containing different carbon sources. We found that transcriptional changes of key metabolic genes during *M. tuberculosis* growth arrest were independent of stress signal and carbon source. Thus, *M. tuberculosis* persistence shares critical metabolic features with bacterial and yeast sporulation, plant seed formation and animal hibernation. Our results lead to the novel view that the metabolic changes of *M. tuberculosis* are part of a developmental decision rather than a response to changed nutrient availability.

## Results and discussion

To assess carbon flow distribution during the establishment of persistent infection, we used a model of respiratory infection of mice in which *M. tuberculosis* replicates in the lung for about 20 days, followed by stabilization of bacterial numbers due to expression of acquired cell-mediated immunity (Shi *et al*., 2003; 2005). We measured changes of bacterial transcript abundance in the mouse lung using qPCR with samples taken at multiple times post-infection (day 12 through day 100). We then expressed the data as a ratio of abundance at each given time point relative to that measured at day 12 (mid-log growth).

The *in vivo* data are presented below in two sections: (i) central metabolism and fatty acid catabolism and (ii) lipid biosynthesis. Of the lipid biosynthetic genes, we focused on those involved in the synthesis of the major storage compound TAG (Garton *et al*., 2008) and of the major components of the mycobacterial cell wall, such as mycolic acids and multimethyl-branched lipids. At the end of each section, the data are interpreted through a metabolic model of *M. tuberculosis* growth arrest. A scheme showing the main pathways of carbon metabolism and the representative genes in each pathway selected for analysis is presented in Fig. 1 and Table S1.

### *Central metabolism*

*Glycolysis and the pentose phosphate pathway (PPP).* Glucose is oxidized through glycolysis and, to a lesser extent, through the PPP (Jayanthi Bai *et al*., 1975). Glycolysis yields central metabolites such as PEP, pyruvate and acetyl-CoA (AcCoA). PPP generates reducing equivalents for reductive biosynthetic reactions and provides ribose 5-P for nucleotide synthesis. Enumeration of transcripts encoding key glycolytic and PPP enzymes of *M. tuberculosis* showed that most transcripts were downregulated during growth arrest relative to log growth (up to 15-fold decrease at day 30 of infection) (Fig. 2A and B; Table S2). However, two genes encoding phosphofructokinase differed in their response. *pfkA* was downregulated, while *pfkB* was strongly upregulated: the number of *pfkB* transcripts peaked at day 18 (65-fold) and remained high for the remainder of infection (> 30-fold at day 100) (Fig. 2A). Since *pfkB* is a member of the *devR*/*dosR* regulon (Voskuil *et al*., 2003), *pfkB* upregulation agrees with our previous observation that DevR/DosR-regulated genes are induced by expression of immunity in the mouse lung (Shi *et al*., 2003).

Sugars are presumably scarce during infection, and most glycolytic reactions can be reversibly utilized for gluconeogenesis. However, a decreased intracellular concentration of C6 sugars should occur instead, due to, the observed downregulation of most glycolytic genes and the strong upregulation of *pfkB*, whose product catalyses the irreversible and rate-limiting reaction of glycolysis. This scenario is consistent with bacillary growth arrest, since C6 sugars may serve as precursors for macromolecular biosynthesis during growth.

*Fatty acid degradation.* Fatty acids, which are the main source of carbon and energy for *M. tuberculosis* during

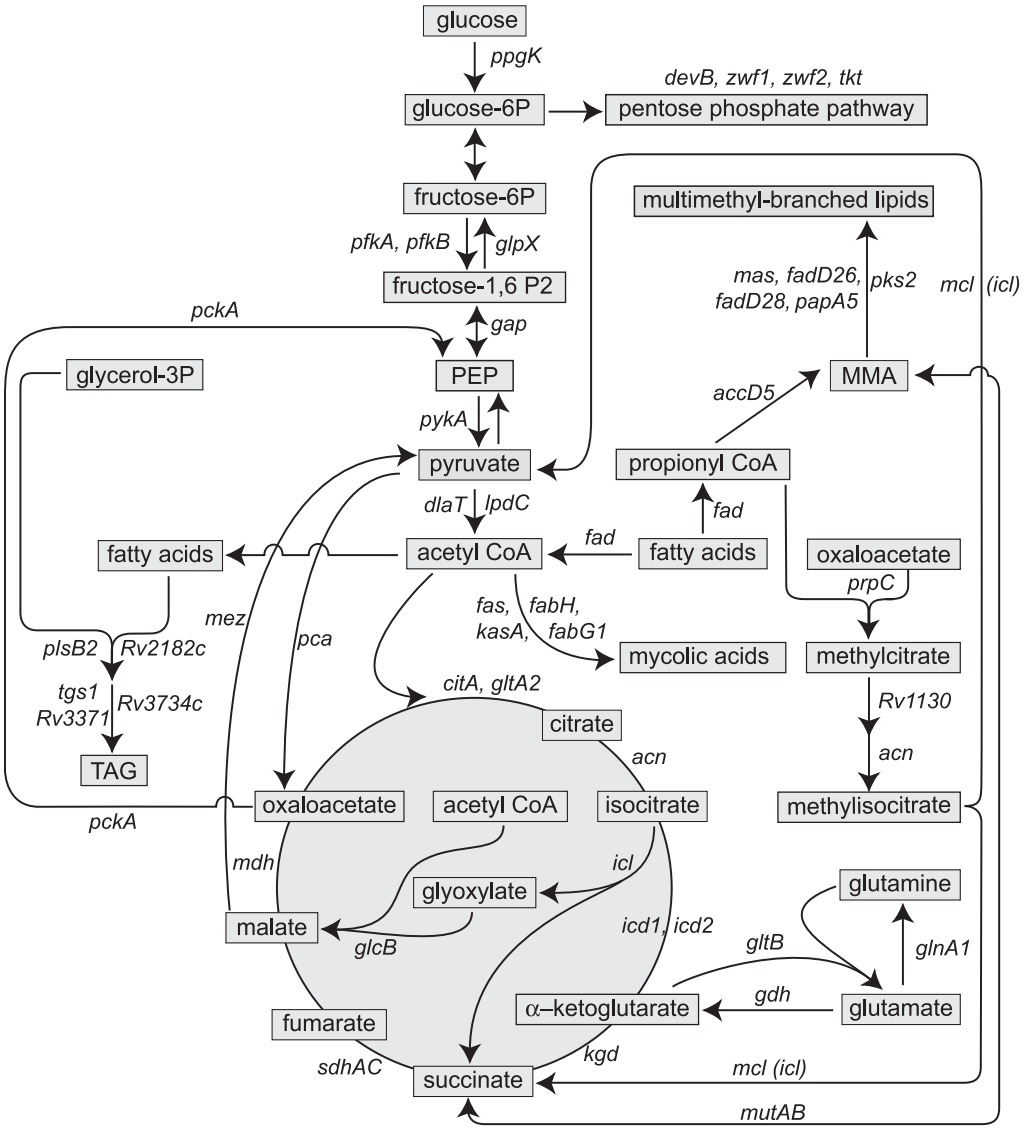


**Fig. 1.** Pathways and genes in central metabolism and lipid metabolism in *M. tuberculosis* analysed in the present work. Gene names or Rv numbering (Cole *et al.*, 1998) are indicated. Abbreviations: PEP, phosphoenolpyruvate; MMA, methylmalonyl-CoA; TAG, triacylglycerol. Lines may represent one or multiple reactions in a pathway. **Fatty acid β-oxidation**: *fadE5* (Rv0244c) and *fadE23* (Rv3140), acyl-CoA dehydrogenase; *fadA4* (Rv1323), acyl-CoA acetyltransferase; *fadB* (Rv0860), fatty acid oxidation protein. **Glycolysis**: *ppgK* (Rv2702), glucokinase; *pfkA* (Rv3110c) and *pfkB* (Rv2029c), phosphofructose kinase; *gap* (Rv1436), glyceraldehyde 3-P dehydrogenase; *pykA* (Rv1617), pyruvate kinase; *dlaT* (Rv2215) and *lpdC* (Rv0462), E2 and E3 components of pyruvate dehydrogenase. **PPP**: *devB* (Rv1445), 6-phosphogluconolactonase; *zwf1* (Rv1121) and *zwf2* (Rv1447c), glucose 6-P 1-dehydrogenase; *tkt* (Rv1449c), transketolase. **TCA cycle**: *citA* (Rv0889c), citrate synthase II; *gltA2* (Rv0896), citrate synthase I; *acn* (Rv1475), aconitase; *icd1* (Rv3339c) and *icld2* (Rv0066c), isocitrate dehydrogenase; *kgd* (Rv1248c), α-ketoglutarate decarboxylase; *sdhA* (Rv3318), flavoprotein of succinate dehydrogenase; *sdhC* (Rv3316), cytochrome B-556 of succinate dehydrogenase; *mdh* (Rv1240), malate dehydrogenase. **Glyoxylate shunt**: *icl* (Rv0467), isocitrate lyase; *glcB* (Rv1837c), malate synthase. **Methylcitrate cycle and methylmalonyl pathway**: *prpDC* (Rv1130–1131), methylcitrate dehydratase and methylcitrate synthase respectively; methylisocitrate lyase (*mcl*) activity is expressed by *icl* (Rv0467); *mutAB* (Rv1942-43), methylmalonyl-CoA mutase, small and large subunit. **Gluconeogenesis**: *mez* (Rv2332), malic enzyme; *pckA* (Rv0211), PEP carboxykinase; *glpX* (Rv1099c), fructose 1,6-bisphosphatase. **Glutamate and glutamine synthesis**: *gltB* (Rv3859), glutamate synthase (large subunit); *glnA1* (Rv2220), glutamine synthetase; *gdh* (Rv2476c), glutamate dehydrogenase. **TAG synthesis**: *plsB2* (Rv2482c), glycerol 3-P acyltransferase; *Rv2182c*, 1-acylglycerol 3-P O-acyltransferase; *tgs1* (Rv3130c), TAG synthase; Rv3734c and Rv3371, TAG synthase. **Mycolic acid synthesis**: *fas* (Rv2524c), fatty acid synthase; *fabH* (Rv0533c), β-ketoacyl-AcpM synthase III; *kasA* (Rv2245), β-ketoacyl-AcpM synthase; *fabG1* (Rv1483), β-ketoacyl-AcpM reductase. **Multimethyl-branched lipid synthesis**: *accD5* (Rv3280), PropCoA carboxylase β chain 5; *mas* (Rv2940), mycocerosic acid synthase; *fadD26* (Rv2930), fatty-acid-CoA ligase; *fadD28* (Rv2941), fatty-acid-CoA synthetase; *papA5* (Rv2939), conserved polyketide synthase; *pks2* (rv3825c), conserved polyketide synthase.

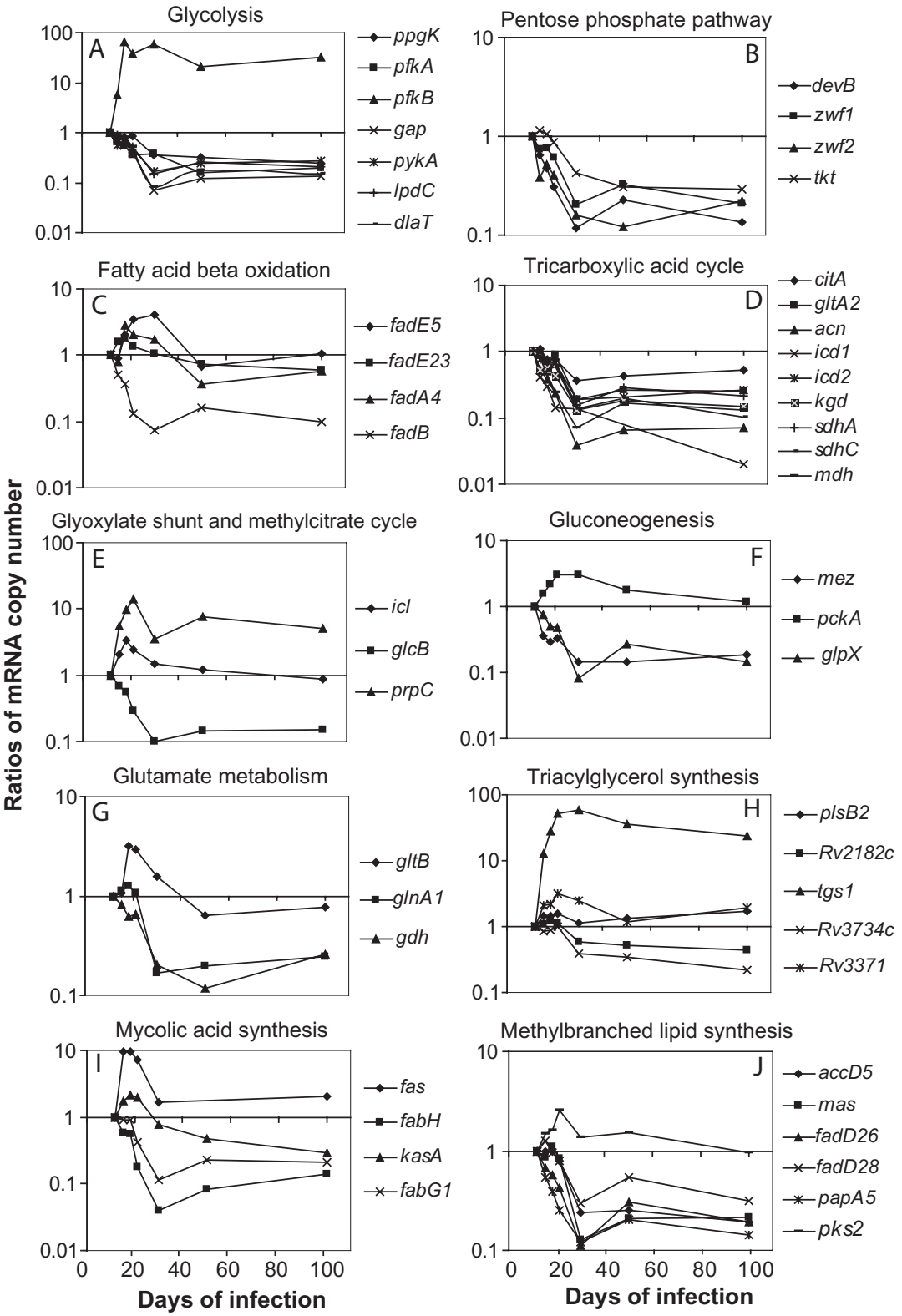


**Fig. 2.** Changes in mRNA levels of *M. tuberculosis* genes involved in central metabolism and lipid metabolism during mouse lung infection. Lungs were harvested from three to four mice at multiple time points (up to day 100) post-infection, as indicated. Total RNA was extracted and qPCR enumeration of bacterial transcripts was performed. Bacterial mRNA copy numbers were normalized to 16S rRNA. Results are shown as ratios of the mean of normalized mRNA copy numbers at each time point relative to the mean of normalized copy numbers at day 12 post-infection. Raw data (means and SD) for each time point are shown in Table S2. Each panel represents the indicated metabolic pathways.

infection, are primarily catabolized via successive rounds of β-oxidation. Even-chain fatty acids are degraded to AcCoA, and odd-chain fatty acids are degraded to both AcCoA and propionyl-CoA (PropCoA). It is likely that tubercle bacilli catabolize a wide range of fatty acids, since they possess a large number of duplicated genes that are annotated as encoding β-oxidation enzymes (Cole *et al*., 1998).

We examined four genes involved in β-oxidation, *fadA4, fadB, fadE5* and *fadE23*, which had previously been reported to be induced *in vivo* (Dubnau *et al*., 2005) or under several stress conditions *in vitro* (Wilson *et al*., 1999; Schnappinger *et al*., 2003; Hampshire *et al*., 2004). We found that the *fadB* transcript decreased > 10-fold by day 30, while *fadE5*, *fadE23* and *fadA4* were moderately upregulated during growth arrest (two- to fourfold induction between days 18 and 30) (Fig. 2C and Table S2). This result shows that individual *fad* genes respond differently *in vivo*, perhaps reflecting specific fatty acid substrates in the infected cell.

*Tricarboxylic acid (TCA) cycle.* AcCoA derived from the catabolism of fatty acids or sugars is assimilated via the TCA cycle, which provides biosynthetic precursors and reducing equivalents for energy generation and biosynthetic reactions. In *M. tuberculosis*, the TCA cycle operates as a variant in which α-ketoglutarate is converted to succinate by an α-ketoglutarate decarboxylase (*kgd*) and succinic semialdehyde dehydrogenase (*gabD1* and *gabD2*) (Tian *et al*., 2005). Transcript levels of key TCA cycle genes, including *kgd*, were downregulated during growth arrest (up to 25-fold by day 30; Fig. 2D and Table S2), implying that the TCA cycle in growth-arrested bacilli functions differently than in growing cells.

*Glyoxylate shunt and methylcitrate cycle. M. tuberculosis* utilizes two additional pathways for assimilating AcCoA and PropCoA from fatty acid and cholesterol catabolism. One is the glyoxylate shunt, which comprises the sequential activities of isocitrate lyase (*icl*) and malate synthase (*glcB*). It converts AcCoA into C4-intermediates while bypassing the decarboxylation steps of the TCA cycle. The second pathway is the methylcitrate cycle. In this cycle PropCoA is converted to pyruvate via three specific enzymatic activities, methylcitrate synthase (*prpC*), methylcitrate dehydratase (*prpD*) and 2-methyl-isocitrate lyase (*icl*) (Munoz-Elias *et al*., 2006). In *M. tuberculosis*, 2-methyl-isocitrate lyase and isocitrate lyase activities are encoded by a single gene (called *icl or icl1, rv0467*) (Gould *et al*., 2006).

Transcript enumeration by qPCR showed that expression of *icl* was moderately induced (up to threefold between days 15 and 30), while *glcB* was downregulated (10-fold) in growth-arrested bacilli. Levels of *prpDC* mRNA peaked (> 10-fold) at day 21 and remained high (fivefold at day 100) (Fig. 2E and Table S2). Thus, three genes involved in the methylcitrate cycle (*prpC*, *prpD* and *icl*) are upregulated. We note that the lack of coordinated regulation of *icl* and *glcB* separates *M. tuberculosis* from other bacteria, including closely related Actinobacteria such as *Corynebacterium glutamicum* (Wendisch *et al*., 1997). We propose that, even though *glcB* is downregulated, the flux through the shunt increases because isocitrate lyase is the key enzyme in the TCA cycle/glyoxylate shunt transition (Walsh and Koshland, 1985).

*Gluconeogenesis.* Growth on fatty acids, TCA cycle intermediates and other substrates that enter the TCA cycle via AcCoA requires the synthesis of glycolytic C3-intermediates, such as PEP and pyruvate, via the decarboxylation of C4-intermediates of the TCA cycle. The enzyme combinations required for C4-decarboxylation and C3-carboxylation vary among bacterial species. *M. tuberculosis* encodes pyruvate carboxylase (*pca*), which catalyses the pyruvate to OAA reaction, the malic enzyme (*mez*) for the malate to pyruvate reaction, and PEP carboxykinase (*pckA*) for the irreversible conversion of OAA to PEP. PEP carboxykinase activity is essential for *M. tuberculosis* growth and persistence in mice (Marrero *et al*., 2010). In addition, gluconeogenesis requires dephosphorylation of fructose 1,6-bisphosphate by a 1,6-bisphosphatase (*glpX*) (Movahedzadeh *et al*., 2004). Of the above genes, only *pckA* was upregulated in tubercle bacilli during mouse lung infection (up to threefold induction between days 18 and 50), as previously observed (Timm *et al*., 2003). Levels of the *pca* transcript were below detection, and transcript levels for *mez* and *glpX* were downregulated (up to 10-fold at day 30, Fig. 2F and Table S2). The combined upregulation of *pckA* and downregulation of *glpX*, which encode enzymes catalysing irreversible reactions, point towards C3-compound synthesis during *M. tuberculosis* growth arrest.

*Glutamate and glutamine synthesis.* To gain insight on how *M. tuberculosis* growth arrest affects carbon flux between carbon and nitrogen metabolism via the TCA cycle intermediate α-ketoglutarate, we probed the expression of genes involved in the metabolism of glutamate, which is one of the most abundant cellular metabolites in tubercle bacilli (Tian *et al*., 2005). Glutamate is synthesized by glutamate synthase (*gltDB*) from α-ketoglutarate and glutamine, the primary product of ammonium assimilation. Glutamine is synthesized by glutamine synthetase, which is encoded by the essential gene *glnA1* (Tullius *et al*., 2003; Harth *et al*., 2005). Glutamate dehydrogenase (*gdh*) can also participate in glutamate metabolism by catalysing the reversible reaction from glutamate to α-ketoglutarate and ammonium.

We found that *glnA1* and *gdh* were downregulated (approximately fivefold) by day 30 (Fig. 2G and Table S2). In contrast, *gltDB* was induced (up to threefold) between days 18 and 30, suggesting that *M. tuberculosis* directs its carbon flux from α-ketoglutarate towards formation of glutamate during growth arrest. This direction of the carbon flux is supported by the decreased expression of *kdg* in the TCA cycle variant (see above). Glutamate may function as a nitrogen reserve to be utilized for bacterial re-growth when environmental conditions become favourable. It may also serve as a 'compatible solute' to keep metabolic enzymes functional under stress conditions (Kempf and Bremer, 1998). Moreover, glutamate contributes to mycobacterial cell wall structure (Harth *et al*., 2000). The observed downregulation of glutamine synthetase (*glnA1*) in non-growing bacilli is consistent with a reduced requirement for glutamine, which is a precursor of the cell wall component poly-L-glutamine (Tullius *et al*., 2003). Thus, the ratio of poly-L-glutamate to poly-L-glutamine in the *M. tuberculosis* cell wall is expected to increase during growth arrest.

### *Metabolic scheme I: accumulation of C3 compounds*

The changes in mRNA abundance reported above suggest that as tubercle bacilli stop replicating, they respond to the decreased demand for energy and biosynthetic precursors by downregulating glycolysis, PPP and the TCA cycle. The resulting reduced synthesis of NADH from central metabolism fits well with the reduced activity of the electron transport chain postulated in our previous work (Shi *et al*., 2005). In the context of decreased TCA cycle activity, C4 compounds (malate and OAA) are mostly generated via the increased activity of the glyoxylate shunt, which also serves an anaplerotic function (Gottschalk, 1985). OAA is then converted to PEP by PEP carboxykinase. Carbon from PropCoA is directed towards pyruvate formation via the methylcitrate cycle. In addition to the above pathways, PEP and pyruvate are formed via the concerted upregulation of glycolytic phosphofructokinase (*pfkB*) and downregulation of gluconeogenic fructose 1,6-bisphosphatase (*glpX*), which would inhibit the late steps of gluconeogenesis. Thus, the flux of carbon during growth arrest of *M. tuberculosis* is expected to be towards the generation of the C3 compounds PEP and pyruvate.

### *Lipid biosynthesis*

To explore the metabolic fate of C3 compounds during growth arrest, we probed two aspects of lipid biosynthesis: (i) synthesis of TAG, a storage lipid implicated in the stress response and long-term survival of *M. tuberculosis* (Daniel *et al*., 2004; Garton *et al*., 2008; Low *et al*., 2009), and (ii) biosynthesis of major cell wall components, such as mycolic acids and multimethyl-branched lipids, which utilizes significant amounts of ATP, reducing power and biosynthetic precursors generated from central metabolism.

*TAG synthesis.* TAGs are synthesized from glycerol 3-P and short- or intermediate-chain acyl primers. Genes involved in synthesis of monoacylglycerol 3-P (*plsB2*) and diacylglycerol 3-P (*rv2182c*) were expressed at an unchanged or slightly reduced (approximately twofold) level during growth arrest (Fig. 2H and Table S2). Of the multiple TAG synthases encoded by *M. tuberculosis*, the TAG synthase encoded by *tgs1* (TGS1) accounts for most of the TAG synthetic activity, at least when examined *in vitro* (Daniel *et al*., 2004; Sirakova *et al*., 2006). This gene, which is regulated by *dosR/devR*, was strongly upregulated in growth-arrested bacilli (20- to 60-fold between days 18 and 100) (Fig. 2H and Table S2), suggesting that TAG accumulates in non-growing bacilli in mouse lungs, as seen with non-growing bacilli *in vitro* (Garton *et al*., 2002). Much smaller changes were seen with other TAG synthase genes: *rv3371* increased and *rv3734* decreased by two- to threefold at day 30.

*Mycolic acid synthesis.* Mycolic acids are long-chain, high-molecular-weight α-alkyl, β-hydroxyl fatty acids that are essential components of the mycobacterial cell wall. They are synthesized by the type I and type II fatty acid synthase systems (FAS-I and FAS-II) (Bhatt *et al*., 2007). FAS-I, which is a single, multi-domain polypeptide encoded by *fas*, mediates *de novo* synthesis of intermediate-length, saturated α-chain of mycolic acids (C26) and synthesis of short-chain fatty-acyl-CoA primers (C16). FAS-II is a multi-enzyme complex that elongates the acyl-CoA primers generated by FAS-I to produce the full-length meromycolate chain of mycolic acids (Bhatt *et al*., 2007). FAS-I and FAS-II are linked by the activity of a β-ketoacyl-AcpM synthase III (*fabH*), which catalyses the condensation between FAS-I acyl-CoA primers and malonyl-AcpM (the product of malonyl-CoA activation by malonyl-CoA:AcpM transacylase). The *fabH* gene product also funnels precursors to FAS-II (Choi *et al*., 2000).

We observed that *fas* (FAS-I system) was upregulated (up to 10-fold) between days 15 and 30 of infection. In the FAS-II system, *kasA*, one of the *kas* operon genes (Gupta and Singh, 2008), was modestly induced (twofold), while expression of the unlinked *fabG1* decreased ~ 10-fold. In addition, *fabH* was strongly downregulated (25-fold) (Fig. 2I and Table S2). The downregulation of *fabH* strongly suggests uncoupling of the FAS-I- and FAS-II-mediated reactions. The potential consequences of such uncoupling on the fate of the FAS-I product and on the structure of the cell wall of non-growing bacilli are dis-

cussed below (*Metabolic scheme II: TAG accumulation and altered cell wall composition*).

*Synthesis of multimethyl-branched lipids.* Multimethyl-branched lipids, which include phthiocerol dimycocerosate (PDIM) and sulpholipids (SL), are uniquely found in the cell envelope of pathogenic mycobacteria, where they have been associated with virulence and modulation of host immune responses (Karakousis *et al*., 2004). These compounds are synthesized by specialized polyketide synthases that elongate straight-chain fatty acids by stepwise addition of short acyl chains (Jackson *et al*., 2007). Precursors for the synthesis of PDIM and SL are straight-chain fatty-acid-acyl primers and methylmalonyl-CoA (MMA), the product of PropCoA activation by a PropCoA carboxylase (Gago *et al*., 2006).

Expression of *accD5*, which encodes the PropCoA carboxylase β chain, was decreased at day 21, concurrent with bacterial growth arrest. Levels of *mutAB*, which encodes the MMA-succinyl-CoA mutase that catalyses the interconversion between MMA and succinyl-CoA (Savvi *et al*., 2008), were below qPCR detection. Genes involved in the synthesis of PDIM were downregulated (4- to 10-fold), while *pks2*, which encodes a polyketide synthase involved in the synthesis of the main sulpholipid SL-1, was moderately upregulated (> 2-fold) by day 30 (Fig. 2J and Table S2). These data are consistent with PDIM synthesis decreasing and, albeit modestly, SL-1 synthesis increasing as tubercle bacilli enter the non-replicative state.

### *Metabolic scheme II: TAG accumulation and altered cell wall composition*

Based on the results reported above, we propose that the strong downregulation (25-fold) of the *fabH* product, which bridges the FAS-I and FAS-II systems during mycolic acid synthesis, leads to uncoupling of the FAS-II system (elongation) from FAS-I (*de novo* synthesis). Consequently, the FAS-I product would be rerouted to other pathways, including TAG synthesis. Indeed, TAG, which is likely produced by *de novo* synthesis (Sirakova *et al*., 2006), accumulates in tubercle bacilli as they stop growing in response to stress *in vitro*, concurrent with decreased fatty acid incorporation into phospholipids and loss of acid-fastness (Deb *et al*., 2009).

Our data are also consistent with the possibility that the cell wall of non-growing tubercle bacilli differs structurally from that of growing bacilli. Once uncoupled from FAS-I, the FAS-II system would elongate the existing meromycolate chain of mycolic acid rather than the newly made FAS-I products. Additionally, the slight upregulation of SL-1 synthetic genes and the concurrent downregulation of PDIM biosynthetic genes suggest that MMA, a precursor for both PDIM and SL-1, could be rerouted from PDIM to SL-1, in agreement with biochemical data showing that blocked synthesis of PDIM leads to increased relative abundance and mass of SL-1 (Jain *et al*., 2007). Peptidoglycan, another cell wall component, is also remodelled in non-replicating tubercle bacilli (Lavollay *et al*., 2008).

### *Carbon flow redistribution*

Collectively, the transcription profiling data presented above lead to a model of carbon flow redistribution during growth arrest of *M. tuberculosis* (Fig. 3). The model predicts that, when tubercle bacilli stop replicating, the main function of central metabolism shifts from providing energy and biosynthetic precursors for bacterial growth to accumulating the storage compounds TAG and glutamate. A key functional shift occurs at the metabolic node that mediates interconversion of C4 compounds and C3 compounds, as seen in the response to stress by many microorganisms (Cortassa *et al*., 2000; Sauer and Eikmanns, 2005). The proposed accumulation of glutamate and TAG is another common theme of metabolic adaptation to stress (Kempf and Bremer, 1998; Murphy, 2001; Alvarez and Steinbuchel, 2002; Waltermann and Steinbuchel, 2005). These storage compounds may serve as carbon and energy sources for long-term persistence and re-growth (Low *et al*., 2009). Aspects of the model, such as upregulation of the glyoxylate shunt and glutamate synthesis, are supported by the results of isotopomer-assisted metabolite analysis of hypoxic adaptation in *Mycobacterium smegmatis* (Tang *et al*., 2009).

### In silico *simulation of* M. tuberculosis *metabolic state during growth and growth arrest*

The metabolic model sketched above is based on transcriptional data obtained from key genes involved in central and lipid metabolism. To begin to assess how transcriptional data correlate with metabolic reactions, we took an *in silico* approach utilizing metabolic networks and flux balance analysis (FBA). With this approach, simulations are performed in which input is nutritional substrate and output is the biomass composition of an *in silico* 'cell'. Biomass is formed through reactions ordered in a metabolic network. The outcome of the simulations is the estimation of fluxes through each reaction in the metabolic network required to obtain maximal biomass. We used these methods to predict metabolic flux patterns in growing and non-growing tubercle bacilli and to assess whether the predicted fluxes were compatible with the bacterial mRNA abundance data obtained *in vivo*. Even though the *in vivo* transcriptional profiling interrogated only selected metabolic pathways, we used a genome-scale metabolic network of *M. tuberculosis* (GSMN-TB)

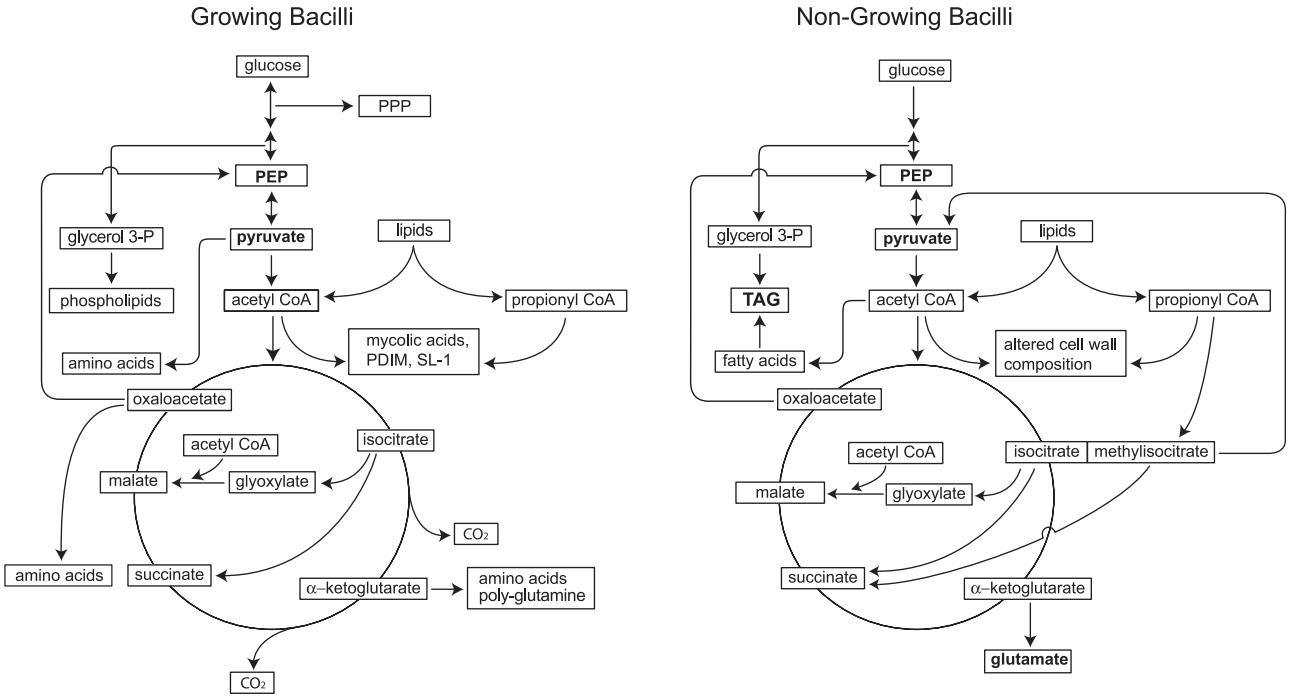


**Fig. 3.** Metabolic model of *M. tuberculosis* infecting the mouse lung. In growing bacilli, carbon from lipid and sugar catabolism is routed via the central metabolism towards generation of energy and biosynthetic precursors required for bacterial growth. Assimilation of AcCoA and PropCoA leads to the synthesis of major cell wall components such as mycolic acids, PDIM and poly-L-glutamine. The glyoxylate shunt is also active, as shown by a requirement for isocitrate lyase activity throughout mouse lung infection (Munoz-Elias and McKinney, 2005). In non-growing bacilli, glycolysis, PPP and TCA cycle are downregulated. AcCoA is preferentially assimilated through the glyoxylate shunt and the gluconeogenetic reactions leading to PEP, while PropCoA is preferentially assimilated via the methylcitrate cycle leading to pyruvate. The resulting formation of PEP and pyruvate, which also results from reduced *de novo* synthesis of sugars, leads to rerouting of carbon flow towards glyceroneogenesis and TAG synthesis. Some AcCoA is also shunted into glutamate biosynthesis. Moreover, uncoupling of FAS-I and FAS-II activities leads to rerouting of FAS-I product towards TAG synthesis and utilization of AcCoA for meromycolate elongation rather than *de novo* synthesis. Together, reduced PDIM synthesis, slightly increased sulpholipid-1 (SL-1) synthesis, reduced poly-L-glutamine synthesis, increased poly-L-glutamate synthesis and meromycolate elongation result in cell wall remodelling. Key intermediates and storage compounds are shown in bold.

[nearly 900 reactions (Beste *et al*., 2007)] for the simulations *in silico*, because regulation of metabolism is a global phenomenon rather than one that depends on particular rate-limiting steps (Fell, 1992).

We first constructed two *in silico* cells by adjusting biomass composition. One cell represented growing *M. tuberculosis*, while the other represented the more minimal cell composition predicted for non-growing *M. tuberculosis* (*Experimental procedures* and Tables S3 and S4A and B). We then used FBA to predict optimal fluxes through each reaction in the network in the models for growing and non-growing cells, when glucose and phospholipid, alone and in combination, were used as carbon sources. Ratios of optimal fluxes were calculated to identify metabolic flux differences between growing and non-growing bacilli. The flux solutions, which are shown in Table S4C–H for all (~ 100) central metabolism reactions in the GSMN-TB network, were then compared with the qPCR data.

For critical pathways of central metabolism, the flux solutions associated with the comparison between growing and non-growing cells were consistent with the *in vivo* data (Fig. 4). First, increased flux in the glyoxylate shunt (Rn 103) and methylcitrate cycle (Rn 82–85) was predicted under all nutritional conditions. This result suggests that increased utilization of these pathways is a response to reduced growth rate rather than to carbon source changes. Second, fluxes through the PPP were predicted to decrease, as expected from the mRNA studies. Third, when glucose and phospholipid were used together as substrate, fluxes through the reactions mediated by PEP carboxykinase (*pckA*) and the malic enzyme (*mez*) (Rn 72 and 101) towards C3-compound formation were predicted to increase. Fourth, the only glycolytic reaction predicted to increase was that mediated by phosphofructokinase (*pfkA,B*) (Rn 41), while the gluconeogenic reaction catalysed by fructose 1,6-bisphosphatase (*glpX*) (Rn 43) was predicted to decrease. The latter two sets of results agree with the PEP and pyruvate synthesis proposed in the metabolic model in Fig. 3.

Differences between *in vivo* data and *in silico* predictions were also observed. In general, a lower degree of concordance was seen between experimental data and *in*

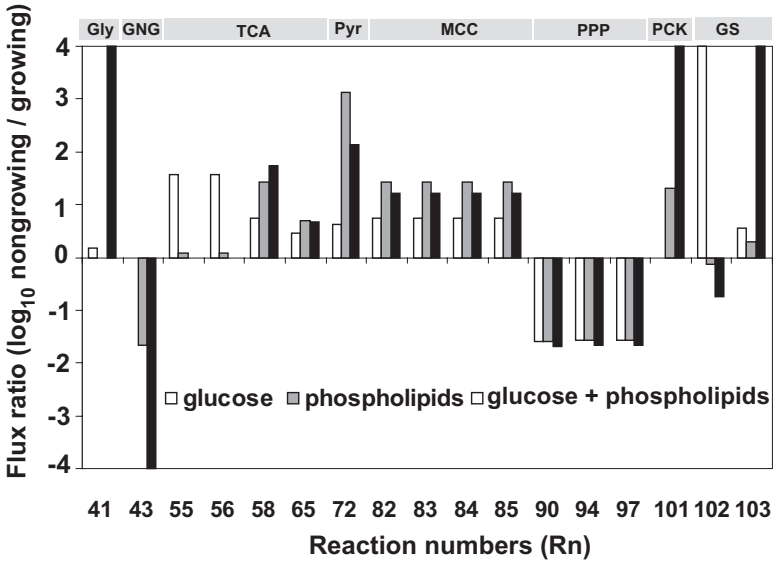


**Fig. 4.** Metabolic flux changes during *M. tuberculosis* growth arrest predicted by *in silico* modelling. FBA of a genome-scale metabolic model of *M. tuberculosis* containing ~ 900 unique reactions (Beste *et al.*, 2007) was conducted. The indicated substrates were used as input, and biomass of growing and non-growing tubercle bacilli cells was used as output (details in Tables S3 and S4A and B). Shown are ratios between the predicted flux values for growing and non-growing cells for 17 central metabolism reactions described in the text. Flux ratio calculations for all central metabolism reactions (~ 100) are shown in Table S4C–H. Positive ratios indicate fluxes in the same direction in growing versus non-growing bacilli, and negative ratios indicate reactions in the opposite direction. Flux ratios that reach the +4/–4 value in the figure have values outside the range shown (see Table S4C–H). Reaction numbers are from the metabolic model (Table S4C–H). Abbreviations: Gly, glycolysis; GNG, gluconeogenesis; Pyr, pyruvate metabolism; TCA, tricarboxylic acid cycle; MCC, methylcitrate cycle; PPP, pentose phosphate pathway; PCK, PEP carboxykinase; GS, glyoxylate shunt.

*silico* fluxes when glucose and phospholipids were used separately. For example, fluxes through several TCA cycle steps (Rn 55, 56, 58, and 65) were predicted to be higher in non-growing bacilli *in silico* (Fig. 4), but the corresponding genes were not upregulated *in vivo*. Other differences involved obtaining the same metabolic outcome *in silico* and *in vivo*, but with different routes/reactions being utilized. For example, the mouse infection data showed upregulation of *icl* (the first gene in the glyoxylate shunt), while *in silico* analysis revealed an increase in flux associated with the second reaction (Rn 103, mediated by malate synthase). Also, non-growing cells showed upregulation of *pckA*, but not *mez*, *in vivo*, while fluxes through both reactions were predicted to increase *in silico*.

In conclusion, the results of the *in silico* simulations were consistent with the main aspects of the metabolic model derived from the qPCR data, although the same metabolic outcome was sometimes obtained via different routes *in silico* and *in vivo*. This result presumably indicates a need for introducing additional constraints *in silico* to fully recapitulate the *in vivo* state.

### *Adaptation of carbon metabolism of* M. tuberculosis *to stress* in vitro

The finding that metabolic shifts accompanying growth arrest were largely independent of nutrient availability *in silico* led us to test experimentally whether these metabolic shifts were related to bacterial growth rate or to nutrient availability. To address this question, we compared transcription profiles associated with growth arrest of *M. tuberculosis* in the mouse lung with those of *M. tuberculosis* cultures subjected to bacteriostatic treatments in media containing different carbon sources.

*Metabolic characteristics of growth-arrested bacilli in enriched culture media.* We first examined whether transcript abundance changes in the metabolic genes examined *in vivo* were also seen when *M. tuberculosis* cells were cultured in standard rich media (containing glucose, fatty acids and amino acids; see *Experimental procedures*) and subjected to either of two bacteriostatic stressors, gradual $O_2$ depletion (Wayne and Hayes, 1996) and treatment with nitric oxide (NO) released from diethylenetriamine/NO (DETA/NO) (Voskuil *et al.*, 2003).

We found a significant overlap in gene expression profiles between non-growing bacilli *in vivo* and *in vitro*. Key carbon metabolic pathways/reactions upregulated in mouse lungs were also induced in growth-arrested cultures (Fig. 5 and Tables S2 and S5A and B). These included glycolysis (*pfkB*), the glyoxylate shunt (*icl*), gluconeogenesis (*pckA*), synthesis of short- to intermediate-chain-length fatty acids (*fas*), elongation of meromycolate of mycolic acid (*kasA*) and synthesis of TAG (*tgs1*) (Fig. 5).

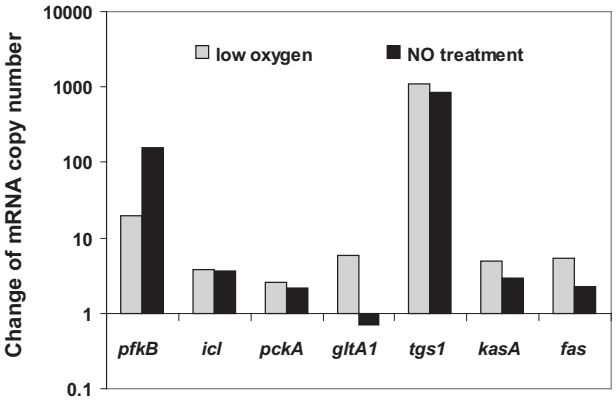


**Fig. 5.** Expression changes of metabolic genes of *M. tuberculosis* during hypoxia and after treatment with NO in cultures grown in enriched media. *M. tuberculosis* cells were cultured in standard Dubos Tween-Albumin medium, and mid-log-phase cultures were subjected to gradual $O_2$ depletion (Wayne model) or treatment with 100 μM DETA/NO. Culture aliquots were harvested at multiple times post-treatment. Transcripts were enumerated by qPCR and normalized to 16S rRNA. Shown are ratios between the means of normalized mRNA copy numbers [at hours 102 or 126 in hypoxia, or after 0.5 h of DETA/NO treatment] and the mean of the mid-log-phase culture data. The hypoxia data are from one of two independent repeats, which gave very similar results (measurements for all genes and time points tested are shown in Table S5A). The NO treatment data were obtained from triplicate samples [ratios for additional genes and time points tested are shown Table S5B; raw data (means and SD) for all genes and time points tested are shown in Table S5C].

The induction of *tgs1* should result in accumulation of TAG in non-growing bacilli. When we tested this possibility in the gradual $O_2$ depletion model by cytological staining and microscopy, we found that hypoxic cultures gradually accumulated neutral lipids while losing acid-fastness (Fig. 6), as previously seen with *M. tuberculosis* cultures subjected to multiple stress conditions (Deb *et al.*, 2009). Accumulation of TAG provides a phenotypic correlate of *tgs1* mRNA increase.

Only two sets of genes showed different profiles under the three conditions (mouse, hypoxia and NO treatment). One pertained to four *fad* genes, which responded differently in the three conditions, suggesting that *fad* gene responses are condition-specific. The other was *prpCD* in the methylcitrate cycle, which was induced during mouse infection and under hypoxia, but not with NO exposure (Figs 2 and 5, and Tables S2 and S5A and B). This result may reflect different levels of the accessory sigma factor E, which regulates the *prpCD* response (Manganelli *et al.*, 2001) under several stress conditions (P. Datta and M.L. Gennaro, unpubl. data).

The observation that the vast majority of metabolic genes probed gave the same response to three bacteriostatic conditions favours the possibility that these responses are associated with growth arrest rather than with nutrient availability (the latter presumably varies

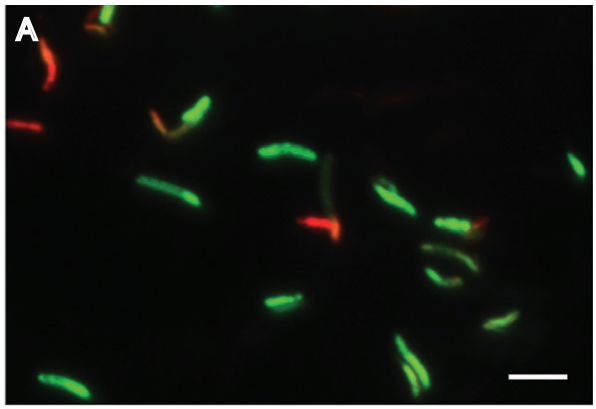


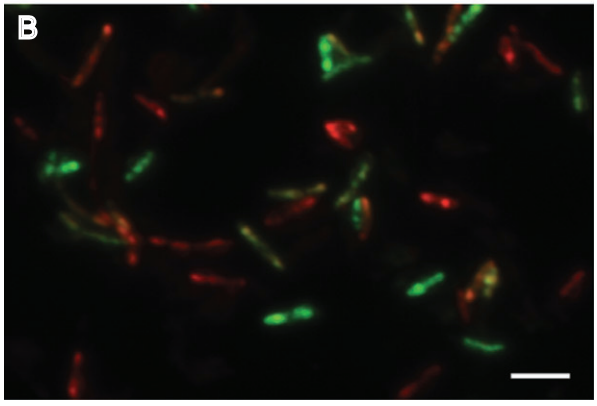


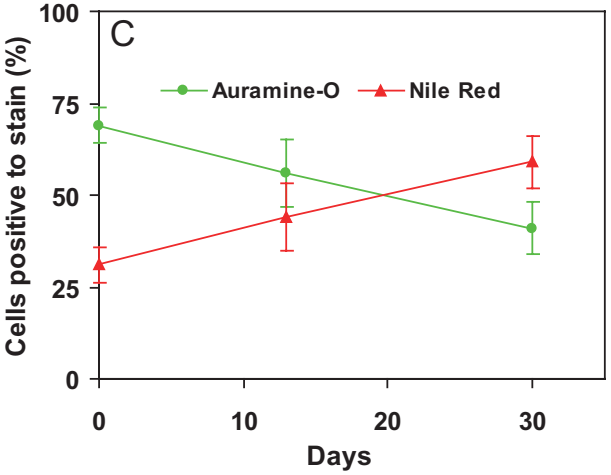


**Fig. 6.** Accumulation of lipid bodies and loss of acid-fastness in *M. tuberculosis* cells during hypoxia.
A and B. *M. tuberculosis* cultures were subjected to gradual $O_2$ depletion (Wayne model). Aliquots from mid-log cultures (A) and cultures at day 30 of the hypoxic time-course (anaerobiosis) (B) were stained for acid-fastness with Auramine-O (green) and for lipid body accumulation with Nile Red (red). Cells were examined by fluorescence microscopy at the same intensity for all samples with Z stacking to get the depth of the scan field. Overlaid images of Auramine-O- and Nile Red-stained cells are shown. Bar = 4 μM.
C. Cells stained with Auramine-O (green line) or Nile Red (red line) were counted from three microscopic fields. Means (and SD) of % stain-positive cells are shown.

**Table 1.** Effects of NO on the transcript levels of selected *M. tuberculosis* central metabolism and lipid metabolism genes in cultures grown with defined carbon sources.

| | Fold change of mRNA copy number | | | | | |
|---|---|---|---|---|---|---|
| | LIM | | | 7H9-S | | |
| Time | *icl* | *pckA* | *tgs1* | *icl* | *pckA* | *tgs1* |
| 0.5 h | 10.2 | 4.7 | 118.0 | 6.3 | 3.0 | 45.2 |
| 1 h | 4.1 | 3.6 | 264.6 | 14.0 | 21.2 | 97.2 |
| 2 h | 1.9 | 1.4 | 268.7 | 10.4 | 12.1 | 60.8 |

*Mycobacterium tuberculosis* cultures were grown in modified Middlebrook 7H9 and LIM minimal medium with defined carbon sources, as described in *Experimental procedures.* Mid-log culture was treated with 100 μM DETA/NO and samples were collected at hours 0.5, 1 and 2 post-treatment. Transcripts were enumerated by qPCR as per Fig. 2 legend. Shown are ratios of means of normalized mRNA copy numbers (from three independent experiments) at the indicated time points post-treatment relative to aerated mid-log growth. 7H9-S, simplified 7H9 medium; LIM, LIM minimal medium.

between the *in vivo* situation and the culture conditions utilized *in vitro*). This possibility was tested by utilizing fatty-acid-free culture media (below).

*Metabolic characteristics of growth-arrested bacilli in media containing defined carbon sources.* We next carried out transcription profiling of *M. tuberculosis* cultures grown in two media containing defined carbon sources but no fatty acid. One culture medium was simplified 7H9 medium in which glucose and glutamate serve as carbon and energy source. The other was LIM minimal medium in which glucose was the sole carbon and energy source (media composition is found in Table S6A and B). Potential sources of fatty acids, such as bovine serum albumin (BSA) and Tween-80, were excluded (see *Experimental procedures*).

When *M. tuberculosis* cultures grown in the above media were treated with bacteriostatic concentrations of NO, we found that key metabolic genes, such as *icl*, *pckA* and *tgs1*, were induced (Table 1). These data clearly establish that the upregulation of pathways, such as the glyoxylate shunt, gluconeogenesis and TAG synthesis, are not necessarily linked with a change of substrate from sugar to fatty acids during infection, but with the change of bacterial growth rate associated with the response to stress.

*Activity of key central metabolic enzymes during growth arrest* in vitro. We also measured changes in enzyme activities occurring during hypoxia to determine how they correlated with expression of the corresponding genes under the same conditions. We first tested activity of three enzymes encoded by genes seen as upregulated in the hypoxic time-course. The activity of isocitrate lyase and PEP carboxykinase increased during hypoxic stress (Fig. 7A–D). The activity of methylcitrate synthase, which is encoded by *prpC*, was much lower than that of citrate synthase (~ 35- to 80-fold) (Table S7), likely reflecting the relative low level of *prpC* expression. We then tested activity of the products of three genes that were downregulated during hypoxia. We found that malate dehydrogenase activity decreased during the hypoxic course (Fig. 7E and F). A decrease was also observed during hypoxic stress for glutamine synthetase activity (~ 10-fold), which was more pronounced than the 5-fold decrease in mRNA abundance of *glnA1*, the major glutamine synthetase gene of *M. tuberculosis* (Tullius *et al.*, 2003; Harth *et al.*, 2005) (Fig. 7G and H). The pattern seen with glutamine synthetase and *glnA1* was also seen with glutamate synthase activity and *gltB* expression. In this case, enzyme activity was low ($< 0.005 \pm 0.001$ mmoles $min^{-1}$ $mg^{-1}$) during logarithmic growth and was further reduced to below detection ($< 0.0001$ mmoles $min^{-1}$ $mg^{-1}$) during hypoxic stress (Table S7). Taken together, we found that the changes in enzyme activity correlated well with changes in RNA abundance with single isoform enzymes.

When multiple enzyme isoforms existed or when genes encoding isoforms of the same enzyme responded differently to the hypoxic stress, comparisons between enzymatic activity and RNA abundance were more complex. We examined two such cases. In one example, the observed reduction in the activity of citrate synthase, which is expressed from *citA* and *gltA2*, tracked changes of mRNA abundance for *citA*, but not for *gltA2* (Fig. 7I and J). In another example, we observed no significant increase in phosphofructokinase activity (which is presumably expressed from *pfkA* and *pfkB*) during hypoxic conditions, even though *pfkB* is strongly induced (up to ~ 100-fold) (Fig. 7K and L). The phosphofructokinase activity, which catalyses the irreversible, rate-limiting step of glycolysis, is highly regulated (Thomas *et al.*, 1972; Doelle, 1975; Kotlarz *et al.*, 1975), and the assay conditions may not reflect critical requirements for activity of this enzyme, such as the concentration of regulatory metabolites or relative oxygen tension.

Collectively, with the exception of phosphofructokinase, the changes in enzyme activities expressed by genes critical to our metabolic model largely support the mRNA abundance data.

## Conclusions

The model proposed in Fig. 3 provides an integrated view of components of the response of *M. tuberculosis* metabolism to stress conditions imposed by host immunity. Key aspects of the model are: (i) the PEP/

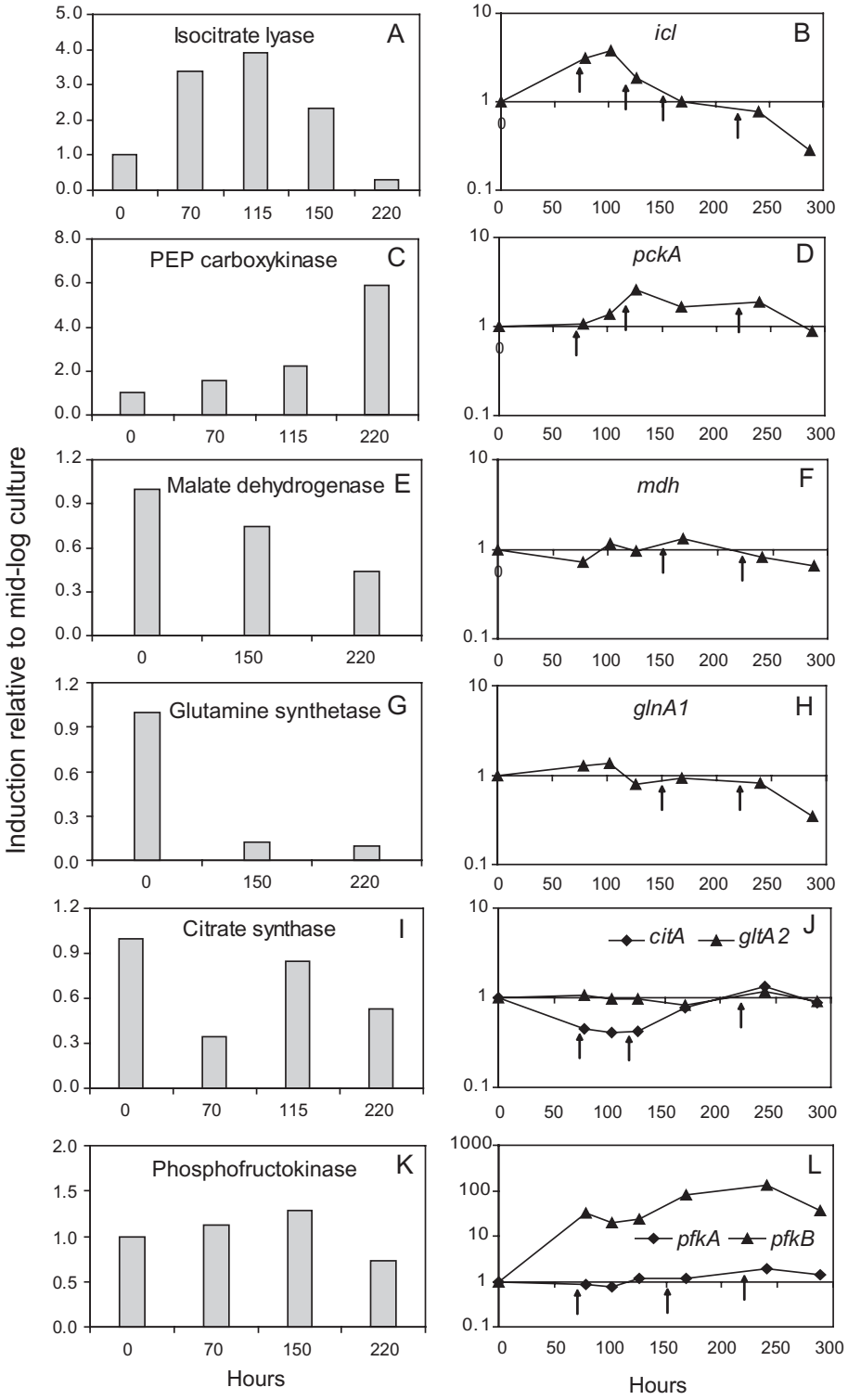


**Fig. 7.** Activity of key metabolic enzymes and corresponding mRNA profiles during hypoxia *in vitro*. Mid-log cultures of *M. tuberculosis* were subjected to gradual $O_2$ depletion (Wayne model). For the enzymatic assays, samples from triplicate cultures were harvested at multiple time points of the hypoxic time-course corresponding to expression changes of the corresponding genes. Left panels: activity results for each enzyme, as indicated. Right panels: copy number changes of the corresponding transcripts. Data are shown as ratios between means of measurements at the indicated time point and those at time 0 (mid-log culture). Raw data (means and SD) for each time point are shown in Table S7.

pyruvate-OAA node is a critical switch of carbon flow distribution, as seen in other bacterial species under stress (Sauer and Eikmanns, 2005), and (ii) carbon flow is rerouted towards formation of storage compounds, such as TAG and glutamate, as also seen in the stress response of many biological systems, as diverse as sporulating bacteria and fungi, plant seeds, and hibernating mammals (Cortassa *et al*., 2000; Murphy, 2001; Alvarez and Steinbuchel, 2002; Waltermann and Steinbuchel, 2005). Thus, our metabolic model characterizes mycobacterial dormancy as a variation of the broader stress–response theme developed in nature.

Our results redefine a central aspect of *M. tuberculosis* biology. Our finding that metabolic activities central to the model are upregulated in response to stress regardless of carbon source or stress signal contradicts the view that these activities are induced in response to change in nutrient availability from sugar to fat (e.g. Honer zu Bentrup and Russell, 2001; Timm *et al*., 2003). The preferential utilization of fatty acids by tubercle bacilli explains the observed requirement for glyoxylate shunt and gluconeogenic genes, such as *icl* and *pckA*, during infection, regardless of growth rate (Munoz-Elias and McKinney, 2005; Marrero *et al*., 2010). Instead, upregulation of the same (and other) metabolic pathways associated with stress-induced bacteriostasis is best interpreted in the context of cell fate decisions (transition from growth to dormancy) rather than as an adaptive response to changed nutrient availability.

A limitation of our metabolic model is that it is largely based on transcript abundance data. However, critical aspects of the model are consistent with *in silico* simulations. Moreover, our experiments with hypoxic cultures show high concordance between expression and activity of key central metabolism enzymes affected during stress-induced bacteriostasis *in vitro*, suggesting that a similar concordance exists also *in vivo*. Furthermore, the accumulation of TAG seen in hypoxic cultures provides a phenotypic correlate to a key prediction of the model. Further ways to test the model will include direct measurements of carbon flux distribution using $^{13}$C-labelled substrates (Eisenreich *et al*., 2010).

In conclusion, we propose that the carbon flow redistribution associated with *M. tuberculosis* growth arrest is a developmental response comparable to that seen with other biological examples of adaptation to stress.

## Experimental procedures

### *Mouse infection*

C57BL/6 mice at 8–10 weeks of age were infected with *M. tuberculosis* $H_{37}$Rv with $\approx 2 \times 10^2$ bacterial colony-forming units (cfu) per mouse, as described (Shi *et al*., 2003). At specified times (days 12, 15, 18, 21, 30, 50 and 100), lungs from three to four mice were harvested and snap-frozen in liquid nitrogen for subsequent RNA extraction.

### *Treatment of* M. tuberculosis *cultures* in vitro

Unless otherwise specified, *M. tuberculosis* $H_{37}$Rv was grown at 37°C in Dubos Tween-Albumin broth (Becton Dickinson), which contains glucose, asparagine and amino acids from a pancreatic digest of casein, and Tween-80 to prevent cell clumping. Tween-80 releases oleic acids that can also be utilized by *M. tuberculosis* as carbon source (Cox *et al*., 1978). Gradual oxygen depletion and treatment with DETA/NO were performed as described (Wayne and Hayes, 1996; Shi *et al*., 2005). For culturing *M. tuberculosis* with defined carbon sources, two additional culture media were used: a modified Middlebrook 7H9 broth with glutamic acid and glucose as carbon source (Table S6A), and LIM minimal medium containing glucose as sole carbon source (Table S6B). Sources of fatty acids were eliminated in the media by replacing the surfactant Tween-80 with the non-metabolizable Tyloxapol and by dispensing of BSA. Mid-log cultures grown in these media were treated with 100 μM DETA/NO and culture aliquots were harvested at hours 0.5, 1 and 2 by centrifugation and snap-frozen in dry-ice/ethanol for subsequent RNA extraction.

### *Enumeration of bacterial transcripts*

RNA extraction, RT-PCR and real-time PCR for bacterial transcript enumeration from infected mouse lungs and cultures were performed, as described (Shi *et al*., 2003). Briefly, total RNA extraction from lungs or cultures utilized rapid mechanical lysis of *M. tuberculosis* in a guanidinium thiocyanate-based buffer. Reverse transcription was performed with gene-specific primers (Table S8) and ThermoScript reverse transcriptase (Invitrogen). Quantification of *M. tuberculosis* mRNAs was carried out by real-time PCR using gene-specific primers, molecular beacons (Table S8) and AmpliTaq Gold polymerase (Applied Biosystems) in a Stratagene Mx4000 thermal cycler. Measurements of mRNA copy numbers per cell were obtained by dividing mRNA copy number by the copy number of 16S rRNA in the same sample, since 16S rRNA copy numbers closely parallel cfu determinations throughout mouse lung infection ($R^2 = 0.9539$) (Shi *et al*., 2003) and in hypoxic cultures *in vitro* (Desjardin *et al*., 2001).

### In silico *simulation of* M. tuberculosis *metabolic pathways at different growth states*

A GSMN-TB (Beste *et al*., 2007) and FBA were used to assess selected metabolic pathways for growing and non-growing bacilli *in silico*. GSMN-TB contains nearly 900 reactions, including the variant TCA cycle containing a-ketoglutarate decarboxylase (*kgd*) and succinic semialdehyde dehydrogenase (Tian *et al*., 2005). In the metabolic model, input was defined as substrate utilized; output was the

generation of biomass of tubercle bacilli. Biomass of 'growing cells' was defined as consisting of DNA, RNA, protein, and major components of the cell wall, as previously described (Beste *et al.*, 2007), while biomass composition for 'non-growing cells' comprised trehalose dimycolate, TAG and polyglutamate/glutamine to reflect a shift towards the minimal cell wall composition deduced from the transcription-derived model in Fig. 3 (detailed biomass composition in Tables S3 and S4A and B). Flux distributions were obtained for maximal biomass production at each growth state by using FBA, as previously described (Beste *et al.*, 2007). Briefly, the FBA method uses linear algebra to calculate the flux in each metabolic reaction of the model that optimizes some 'objective function', in our case, the production of biomass. From the perspective of the FBA analysis, the difference between growing and non-growing cells was the different biomass composition. Therefore, FBA was used to calculate flux values that would optimize production of biomass from growing and non-growing cells. The ratio between these predicted flux values (for growing and non-growing cells) provided a predicted difference of metabolic flux in each reaction between the two states.

### *Fluorescent staining with Auramine-O and Nile Red*

Fluorescent acid-fast staining dye Auramine-O was used in combination with lipid staining dye Nile Red (9-Diethylamino-5H-benzo-α-phenoxazine-5-one). *M. tuberculosis* cultures were taken at multiple time points during hypoxia and heat-killed prior to staining. About 300 μl of cell suspensions were added onto a poly-lysine-coated chambered borosilicate cover glass system and incubated for 30 min at room temperature. After removing excess cell suspension, chambers were air-dried before staining. Acid-fast staining was performed by using Mycobacteria Fluorescent stain kit (Fluka). Briefly, each chamber was filled with 0.3% fluorescent Auramine-O (in 3% phenol solution), incubated in the dark for 15 min, washed with distilled water and treated with decolorizing solution for 2 min. After washing with distilled waster, cells were stained with Nile Red dye (10 μg $ml^{-1}$ in ethanol), incubated in the dark for 15 min, washed with distilled water, treated with counterstain (0.1% potassium permanganate) for 3 min, washed with distilled waster and air-dried. Each chamber was examined with 100 × oil immersion lens using a fluorescent microscope AXIOVERT 200 M (Zeiss). The filter sets used for visualization of cells stained with Auramine-O and Nile Red were Fluorescein (excitation wavelength 475 nm and emission wavelength 530 nm) and Texas Red (excitation wavelength 590 and emission wavelength 630 nm) respectively. Scanned images were analysed and projected by using the OPEN LAB software (Perkin Elmer).

### *Preparation of cell-free extracts and enzyme assays*

*Mycobacterium tuberculosis* was grown to either mid-log phase with an approximate $OD_{580}$ of 0.4 under aerobic conditions and to multiple time points of non-replicating persistence following gradual oxygen depletion in 500 ml flasks. Cultures were harvested by placing them on ice for 2 h and then washing them twice by centrifugation with cold 10 mM phosphate buffer (pH 7.0) containing 0.05% Tween-80. Cells were disrupted in 100 mM phosphate buffer (pH 7.0) containing 1 mM ethylenediaminetetraacetic acid (EDTA), 1 mM dithiothreitol (DTT) and 1 mM phenylmethylsulphonyl fluoride (PMSF) using a Mini-Bead Beater (Bio Spec Products, Bartlesville, OK) with six repetitions of 30 s bursts with cooling on ice between each cycle. Extracts were clarified by centrifugation, and they were sterilized by filtration through a 0.45 μm pore SpinX filter (Corning, New York). The protein concentration was determined with Bio-Rad protein assay reagents (Bio-Rad Laboratories, Hercules, CA, USA).

*Isocitrate lyase.* Isocitrate lyase activity was measured as the amount of glyoxylphenylhydrozone produced from glyoxylate (Hoyt *et al.*, 1991). Fifty micrograms of cell extract protein was added to a cuvette containing 50 mM MOPS buffer (pH 7.5), 5 mM $MgCl_2$ and 4 mM phenylhydrazine hydrochloride. The reaction was started with the addition of trisodium isocitrate to 2 mM, and the absorbance at 324 nm monitored. A control reaction without isocitrate was subtracted as background. An extinction coefficient $1.7 \times 10^4$ $M^{-1}$ $cm^{-1}$ was used to calculate the rate of glyoxylate phenylhydrazone formation.

*PEP carboxykinase.* GTP-dependent PEP carboxykinase was measured with a modified protocol (Mukhopadhyay *et al.*, 2001). Fifty micrograms of cell extract protein was added to a reaction mix containing 200 mM HEPES buffer (pH 7.2), 200 μM $MnCl_2$, 4 mM $MgCl_2$, 10 mM PEP, 100 mM $NaHCO_3$, 200 μM NADH and 3 units of malic dehydrogenase from *Thermus flavus*. The reaction was initiated with the addition of GDP to 2 mM and followed by measuring absorbance at 340 nm. An extinction coefficient of 6223 $M^{-1}$ $cm^{-1}$ was used to calculate the rates of NADH oxidation. A control reaction without PEP was included and subtracted as background.

*Malate dehydrogenase.* Malate dehydrogenase activity was measured by the oxidation of NADH in the presence of OAA according to published protocol with minor modifications (Tian *et al.*, 2005). Reaction mixture contains 50 μg of protein, 50 mM HEPES (pH 8.0), 0.4 mM NADH and 0.4 mM OAA. A control reaction without OAA was included and subtracted as background.

*Citrate synthase.* The assay was carried out according to published protocols (Munoz-Elias *et al.*, 2006). Briefly, 50 μg of cell extract protein was added to a 1 ml cuvette containing 50 mM HEPES buffer (pH 8.0), 100 μM 5,5-dithiobis-(2-nitrobenozate) and 400 μM OAA (pH 8.0). The reaction was initiated with the addition of AcCoA to 70 μM and thionitrobenzene formation was followed by measuring absorbance at 412 nm. An extinction coefficient of 13 600 $M^{-1}$ $cm^{-1}$ was used to calculate the rates. A control reaction without OAA was subtracted as background.

*Methylcitrate synthase.* The assay for methylcitrate synthase activity was the same as for citrate synthase with the exception that AcCoA was replaced with PropCoA.

*Phosphofructokinase.* Phosphofructokinase activity measurement was based on an assay involving aldolase, triose phosphate isomerase and glycerol phosphate dehydrogenase (Alves *et al*., 1997). Fifty micrograms of cell extract protein was added to a reaction mix (pH 7.5) containing 50 mM Tris, 5 mM $MgCl_2$, 3 mM $NH_4Cl$, 1 mM KCl, 7 mM fructose 6-P, 160 μM NADH, 1 unit of fructose bisphosphate aldolase, 5 units of 3-P isomerase and 1 unit of α-glycerol 3-P dehydrogenase. The reaction was initiated with the addition of ATP to 2.5 mM, and NADPH oxidation was monitored by measuring the absorbance at 340 nm. A control reaction without 6-P fructose was included and subtracted as background.

*Glutamate synthase.* The assay was carried out according to published protocols (McCarthy, 1983). Fifty micrograms of cell extract protein was added to a reaction mix containing 50 mM HEPES buffer (pH 8.0), 5 mM glutamine and 160 mM NADH. NADH oxidation was measured by monitoring absorbance at 340 nm. A control reaction without glutamine acid was included and subtracted as background.

*Glutamine synthetase.* The assay measures production of γ-glutamylhydroxamate by glutamine synthetase (Tullius *et al*., 2001). Components were added to a final concentration of 20 mM Imidazole (pH 7.0), 20 mM arsenate, 60 mM hydroxylamine, 1 mM $MnCl_2$, 400 mM ADP and 50 μg of cell extract protein. The reaction was initiated with the addition of alpha-ketoglutarate to 5 mM. At 30 min intervals a 500 μl sample was removed and added to 125 μl of Stop Solution (8% w/v trichloroacetic acid, 3.3% w/v $FeCl_3$ and 2 N HCl). The absorbance at 540 nm was measured and compared with a standard curve.

## Acknowledgements

We thank Ron LaCourse for mouse infections; Michelle Thissen for technical help with the enzyme assays; Gyanu Lamichhane, Lenny Mindich, Issar Smith and Xilin Zhao for critical reading of this manuscript. We give special thanks to Karl Drlica for the generous contribution of his time to discussing this work. L.S. is the recipient of a CFAR grant from New York University. C.P. is the recipient of a scholarship from the NIH Fogarty International Center. The work was supported by grants from the NIAID (R.J.N., L.S. and M.L.G.), the Medical Research Services of the US Department of Veterans Affairs (C.D.S.), the Biotechnology and Biological Sciences Research Council (J.J.McF.) and the Futura Foundation (M.L.G.).

## References

Alvarez, H.M., and Steinbuchel, A. (2002) Triacylglycerols in prokaryotic microorganisms. *Appl Microbiol Biotechnol* **60:** 367–376.

Alves, A.M., Euverink, G.J., Bibb, M.J., and Dijkhuizen, L. (1997) Identification of ATP-dependent phosphofructokinase as a regulatory step in the glycolytic pathway of the actinomycete *Streptomyces coelicolor* A3(2). *Appl Environ Microbiol* **63:** 956–961.

Beste, D.J., Hooper, T., Stewart, G., Bonde, B., Avignone-Rossa, C., Bushell, M.E., *et al*. (2007) GSMN-TB: a web-based genome-scale network model of *Mycobacterium tuberculosis* metabolism. *Genome Biol* **8:** R89.

Bhatt, A., Molle, V., Besra, G.S., Jacobs, W.R., Jr, and Kremer, L. (2007) The *Mycobacterium tuberculosis* FAS-II condensing enzymes: their role in mycolic acid biosynthesis, acid-fastness, pathogenesis and in future drug development. *Mol Microbiol* **64:** 1442–1454.

Bishai, W. (2000) Lipid lunch for persistent pathogen. *Nature* **406:** 683–685.

Bloch, H., and Segal, W. (1956) Biochemical differentiation of *Mycobacterium tuberculosis* grown *in vivo* and *in vitro*. *J Bacteriol* **72:** 132–141.

Brennan, P.J. (2003) Structure, function, and biogenesis of the cell wall of *Mycobacterium tuberculosis*. *Tuberculosis (Edinb)* **83:** 91–97.

Choi, K.H., Kremer, L., Besra, G.S., and Rock, C.O. (2000) Identification and substrate specificity of beta-ketoacyl (acyl carrier protein) synthase III (mtFabH) from *Mycobacterium tuberculosis*. *J Biol Chem* **275:** 28201–28207.

Cole, S.T., Brosch, R., Parkhill, J., Garnier, T., Churcher, C., Harris, D., *et al*. (1998) Deciphering the biology of *Mycobacterium tuberculosis* from the complete genome sequence. *Nature* **393:** 537–544.

Collins, D.M., Wilson, T., Campbell, S., Buddle, B.M., Wards, B.J., Hotter, G., and De Lisle, G.W. (2002) Production of avirulent mutants of *Mycobacterium bovis* with vaccine properties by the use of illegitimate recombination and screening of stationary-phase cultures. *Microbiology* **148:** 3019–3027.

Cortassa, S., Aon, J.C., Aon, M.A., and Spencer, F.T. (2000) Dynamics of metabolism and its interactions with gene expression during sporulation in *Saccharomyces cerevisiae*. In *Advance in Microbial Physiology*. Poole, R.K. (ed.). San Diego, San Francisco, New York, Boston, London, Sydney, Tokyo: Academic Press, pp. 75–115.

Cox, F.R., Slack, C.E., Cox, M.E., Pruden, E.L., and Martin, J.R. (1978) Rapid Tween 80 hydrolysis test for mycobacteria. *J Clin Microbiol* **7:** 104–105.

Daniel, J., Deb, C., Dubey, V.S., Sirakova, T.D., Abomoelak, B., Morbidoni, H.R., and Kolattukudy, P.E. (2004) Induction of a novel class of diacylglycerol acyltransferases and triacylglycerol accumulation in *Mycobacterium tuberculosis* as it goes into a dormancy-like state in culture. *J Bacteriol* **186:** 5017–5030.

Deb, C., Lee, C.M., Dubey, V.S., Daniel, J., Abomoelak, B., Sirakova, T.D., *et al*. (2009) A novel *in vitro* multiple-stress dormancy model for *Mycobacterium tuberculosis* generates a lipid-loaded, drug-tolerant, dormant pathogen. *PLoS ONE* **4:** e6077.

Desjardin, L.E., Hayes, L.G., Sohaskey, C.D., Wayne, L.G., and Eisenach, K.D. (2001) Microaerophilic induction of the alpha-crystallin chaperone protein homologue (hspX) mRNA of *Mycobacterium tuberculosis*. *J Bacteriol* **183:** 5311–5316.

Doelle, H.W. (1975) ATP-sensitive and ATP-insensitive phosphofructokinase in *Escherichia coli* K-12. *Eur J Biochem* **50:** 335–342.

Dubnau, E., Chan, J., Mohan, V.P., and Smith, I. (2005) responses of *mycobacterium tuberculosis* to growth in the mouse lung. *Infect Immun* **73:** 3754–3757.

Eisenreich, W., Dandekar, T., Heesemann, J., and Goebel, W. (2010) Carbon metabolism of intracellular bacterial pathogens and possible links to virulence. *Nat Rev* **8:** 401–412.

Fell, D.A. (1992) Metabolic control analysis: a survey of its theoretical and experimental development. *Biochem J* **286** (Part 2)**:** 313–330.

Gago, G., Kurth, D., Diacovich, L., Tsai, S.C., and Gramajo, H. (2006) Biochemical and structural characterization of an essential acyl coenzyme A carboxylase from *Mycobacterium tuberculosis*. *J Bacteriol* **188:** 477–486.

Garton, N.J., Christensen, H., Minnikin, D.E., Adegbola, R.A., and Barer, M.R. (2002) Intracellular lipophilic inclusions of mycobacteria *in vitro* and *in sputum*. *Microbiology* **148:** 2951–2958.

Garton, N.J., Waddell, S.J., Sherratt, A.L., Lee, S.M., Smith, R.J., Senner, C., *et al*. (2008) Cytological and transcript analyses reveal fat and lazy persister-like bacilli in tuberculous sputum. *PLoS Med* **5:** e75.

Gottschalk, G. (1985) *Bacterial Metabolism*, 2nd edn. New York: Springer-Verlag.

Gould, T.A., van de Langemheen, H., Munoz-Elias, E.J., McKinney, J.D., and Sacchettini, J.C. (2006) Dual role of isocitrate lyase 1 in the glyoxylate and methylcitrate cycles in *Mycobacterium tuberculosis*. *Mol Microbiol* **61:** 940–947.

Gupta, N., and Singh, B.N. (2008) Deciphering *kas* operon locus in *Mycobacterium aurum* and genesis of a recombinant strain for rational-based drug screening. *J Appl Microbiol* **105:** 1703–1710.

Hampshire, T., Soneji, S., Bacon, J., James, B.W., Hinds, J., Laing, K., *et al*. (2004) Stationary phase gene expression of *Mycobacterium tuberculosis* following a progressive nutrient depletion: a model for persistent organisms? *Tuberculosis (Edinb)* **84:** 228–238.

Harth, G., Zamecnik, P.C., Tang, J.Y., Tabatadze, D., and Horwitz, M.A. (2000) Treatment of *Mycobacterium tuberculosis* with antisense oligonucleotides to glutamine synthetase mRNA inhibits glutamine synthetase activity, formation of the poly-L-glutamate/glutamine cell wall structure, and bacterial replication. *Proc Natl Acad Sci USA* **97:** 418–423.

Harth, G., Maslesa-Galic, S., Tullius, M.V., and Horwitz, M.A. (2005) All four *Mycobacterium tuberculosis glnA* genes encode glutamine synthetase activities but only GlnA1 is abundantly expressed and essential for bacterial homeostasis. *Mol Microbiol* **58:** 1157–1172.

Honer zu Bentrup, K., and Russell, D.G. (2001) Mycobacterial persistence: adaptation to a changing environment. *Trends Microbiol* **9:** 597–605.

Hoyt, J.C., Johnson, K.E., and Reeves, H.C. (1991) Purification and characterization of *Acinetobacter calcoaceticus* isocitrate lyase. *J Bacteriol* **173:** 6844–6848.

Jackson, M., Stadthagen, G., and Gicquel, B. (2007) Long-chain multiple methyl-branched fatty acid-containing lipids of *Mycobacterium tuberculosis*: biosynthesis, transport, regulation and biological activities. *Tuberculosis (Edinb)* **87:** 78–86.

Jain, M., Petzold, C.J., Schelle, M.W., Leavell, M.D., Mougous, J.D., Bertozzi, C.R., *et al*. (2007) Lipidomics reveals control of *Mycobacterium tuberculosis* virulence lipids via metabolic coupling. *Proc Natl Acad Sci USA* **104:** 5133–5138.

Jayanthi Bai, N., Ramachandra Pai, M., Suryanarayana Murthy, P., and Venkitasubramanian, T.A. (1975) Pathways of carbohydrate metabolism in *mycobacterium tuberculosis* H37Rv1. *Can J Microbiol* **21:** 1688–1691.

Karakousis, P.C., Bishai, W.R., and Dorman, S.E. (2004) *Mycobacterium tuberculosis* cell envelope lipids and the host immune response. *Cell Microbiol* **6:** 105–116.

Kempf, B., and Bremer, E. (1998) Uptake and synthesis of compatible solutes as microbial stress responses to high-osmolality environments. *Arch Microbiol* **170:** 319–330.

Kotlarz, D., Garreau, H., and Buc, H. (1975) Regulation of the amount and of the activity of phosphofructokinases and pyruvate kinases in *Escherichia coli*. *Biochim Biophys Acta* **381:** 257–268.

Lavollay, M., Arthur, M., Fourgeaud, M., Dubost, L., Marie, A., Veziris, N., *et al*. (2008) The peptidoglycan of stationary-phase *Mycobacterium tuberculosis* predominantly contains cross-links generated by L,D-transpeptidation. *J Bacteriol* **190:** 4360–4366.

Liu, K., Yu, J., and Russell, D.G. (2003) *pckA*-deficient *Mycobacterium bovis* BCG shows attenuated virulence in mice and in macrophages. *Microbiology* **149:** 1829–1835.

Low, K.L., Srinivasa Rao, P.S., Shui, G., Bendt, A.K., Pethe, K., Dick, T., and Wenk, M.R. (2009) Triacylglycerol utilization is required for the re-growth of *in vitro* hypoxic non-replicating *Mycobacterium bovis Bacillus* Calmette-Guerin. *J Bacteriol* **191:** 5037–5043.

McCarthy, C.M. (1983) Continuous culture of *Mycobacterium avium* limited for ammonia. *Am Rev Respir Dis* **127:** 193–197.

McKinney, J.D., Honer zu Bentrup, K., Munoz-Elias, E.J., Miczak, A., Chen, B., Chan, W.T., *et al*. (2000) Persistence of *Mycobacterium tuberculosis* in macrophages and mice requires the glyoxylate shunt enzyme isocitrate lyase. *Nature* **406:** 735–738.

Manganelli, R., Voskuil, M.I., Schoolnik, G.K., and Smith, I. (2001) The *Mycobacterium tuberculosis* ECF sigma factor sigmaE: role in global gene expression and survival in macrophages. *Mol Microbiol* **41:** 423–437.

Marrero, J., Rhee, K.Y., Schnappinger, D., Pethe, K., and Ehrt, S. (2010) Gluconeogenic carbon flow of tricarboxylic acid cycle intermediates is critical for *Mycobacterium tuberculosis* to establish and maintain infection. *Proc Natl Acad Sci USA* **107:** 9819–9824.

Movahedzadeh, F., Rison, S.C., Wheeler, P.R., Kendall, S.L., Larson, T.J., and Stoker, N.G. (2004) The *Mycobacterium tuberculosis* Rv1099c gene encodes a GlpX-like class II fructose 1,6-bisphosphatase. *Microbiology* **150:** 3499–3505.

Mukhopadhyay, B., Concar, E.M., and Wolfe, R.S. (2001) A GTP-dependent vertebrate-type phosphoenolpyruvate carboxykinase from *Mycobacterium smegmatis*. *J Biol Chem* **276:** 16137–16145.

Munoz-Elias, E.J., and McKinney, J.D. (2005) *Mycobacterium tuberculosis* isocitrate lyases 1 and 2 are jointly required for *in vivo* growth and virulence. *Nat Med* **11:** 638–644.

Munoz-Elias, E.J., Upton, A.M., Cherian, J., and McKinney, J.D. (2006) Role of the methylcitrate cycle in *Mycobacterium tuberculosis* metabolism, intracellular growth, and virulence. *Mol Microbiol* **60:** 1109–1122.

Murphy, D.J. (2001) The biogenesis and functions of lipid bodies in animals, plants and microorganisms. *Prog Lipid Res* **40:** 325–438.

Russell, D.G., Cardona, P.J., Kim, M.J., Allain, S., and Altare, F. (2009) Foamy macrophages and the progression of the human tuberculosis granuloma. *Nat Immunol* **10:** 943–948.

Sassetti, C.M., and Rubin, E.J. (2003) Genetic requirements for mycobacterial survival during infection. *Proc Natl Acad Sci USA* **100:** 12989–12994.

Sauer, U., and Eikmanns, B.J. (2005) The PEP-pyruvate-oxaloacetate node as the switch point for carbon flux distribution in bacteria. *FEMS Microbiol Rev* **29:** 765–794.

Savvi, S., Warner, D.F., Kana, B.D., McKinney, J.D., Mizrahi, V., and Dawes, S.S. (2008) Functional characterization of a vitamin B12-dependent methylmalonyl pathway in *Mycobacterium tuberculosis*: implications for propionate metabolism during growth on fatty acids. *J Bacteriol* **190:** 3886–3895.

Schnappinger, D., Ehrt, S., Voskuil, M.I., Liu, Y., Mangan, J.A., Monahan, I.M., *et al*. (2003) Transcriptional adaptation of *mycobacterium tuberculosis* within macrophages: insights into the phagosomal environment. *J Exp Med* **198:** 693–704.

Shi, L., Jung, Y.J., Tyagi, S., Gennaro, M.L., and North, R.J. (2003) Expression of Th1-mediated immunity in mouse lungs induces a *Mycobacterium tuberculosis* transcription pattern characteristic of nonreplicating persistence. *Proc Natl Acad Sci USA* **100:** 241–246.

Shi, L., Sohaskey, C.D., Kana, B.D., Dawes, S., North, R.J., Mizrahi, V., and Gennaro, M.L. (2005) Changes in energy metabolism of *Mycobacterium tuberculosis* in mouse lung and under *in vitro* conditions affecting aerobic respiration. *Proc Natl Acad Sci USA* **102:** 15629–15634.

Sirakova, T.D., Dubey, V.S., Deb, C., Daniel, J., Korotkova, T.A., Abomoelak, B., and Kolattukudy, P.E. (2006) Identification of a diacylglycerol acyltransferase gene involved in accumulation of triacylglycerol in *Mycobacterium tuberculosis* under stress. *Microbiology* **152:** 2717–2725.

Tang, Y.J., Shui, W., Myers, S., Feng, X., Bertozzi, C., and Keasling, J.D. (2009) Central metabolism in *Mycobacterium smegmatis* during the transition from O2-rich to O2-poor conditions as studied by isotopomer-assisted metabolite analysis. *Biotechnol Lett* **31:** 1233–1240.

Thomas, A.D., Doelle, H.W., Westwood, A.W., and Gordon, G.L. (1972) Effect of oxygen on several enzymes involved in the aerobic and anaerobic utilization of glucose in *Escherichia coli*. *J Bacteriol* **112:** 1099–1105.

Tian, J., Bryk, R., Itoh, M., Suematsu, M., and Nathan, C. (2005) Variant tricarboxylic acid cycle in *Mycobacterium tuberculosis*: identification of alpha-ketoglutarate decarboxylase. *Proc Natl Acad Sci USA* **102:** 10670–10675.

Timm, J., Post, F.A., Bekker, L.G., Walther, G.B., Wainwright, H.C., Manganelli, R., *et al*. (2003) Differential expression of iron-, carbon-, and oxygen-responsive mycobacterial genes in the lungs of chronically infected mice and tuberculosis patients. *Proc Natl Acad Sci USA* **100:** 14321–14326.

Tullius, M.V., Harth, G., and Horwitz, M.A. (2001) High extracellular levels of *Mycobacterium tuberculosis* glutamine synthetase and superoxide dismutase in actively growing cultures are due to high expression and extracellular stability rather than to a protein-specific export mechanism. *Infect Immun* **69:** 6348–6363.

Tullius, M.V., Harth, G., and Horwitz, M.A. (2003) Glutamine synthetase GlnA1 is essential for growth of *Mycobacterium tuberculosis* in human THP-1 macrophages and guinea pigs. *Infect Immun* **71:** 3927–3936.

Voskuil, M.I., Schnappinger, D., Visconti, K.C., Harrell, M.I., Dolganov, G.M., Sherman, D.R., and Schoolnik, G.K. (2003) Inhibition of respiration by nitric oxide induces a *Mycobacterium tuberculosis* dormancy program. *J Exp Med* **198:** 705–713.

Walsh, K., and Koshland, D.E., Jr (1985) Branch point control by the phosphorylation state of isocitrate dehydrogenase. A quantitative examination of fluxes during a regulatory transition. *J Biol Chem* **260:** 8430–8437.

Waltermann, M., and Steinbuchel, A. (2005) Neutral lipid bodies in prokaryotes: recent insights into structure, formation, and relationship to eukaryotic lipid depots. *J Bacteriol* **187:** 3607–3619.

Wayne, L.G., and Hayes, L.G. (1996) An *in vitro* model for sequential study of shiftdown of *Mycobacterium tuberculosis* through two stages of nonreplicating persistence. *Infect Immun* **64:** 2062–2069.

Wendisch, V.F., Spies, M., Reinscheid, D.J., Schnicke, S., Sahm, H., and Eikmanns, B.J. (1997) Regulation of acetate metabolism in *Corynebacterium glutamicum*: transcriptional control of the isocitrate lyase and malate synthase genes. *Arch Microbiol* **168:** 262–269.

Wheeler, P.R., and Ratledge, C. (1994) Metabolism of *Mycobacterium tuberculosis*. In *Tuberculosis: Pathogenesis, Protection, and Control*. Bloom, B.R.E. (ed.). Washington, DC: American Society for Microbiology Press, pp. 353–385.

Wilson, M., DeRisi, J., Kristensen, H.H., Imboden, P., Rane, S., Brown, P.O., and Schoolnik, G.K. (1999) Exploring drug-induced alterations in gene expression in *Mycobacterium tuberculosis* by microarray hybridization. *Proc Natl Acad Sci USA* **96:** 12833–12838.

Zhang, Y. (2004) Persistent and dormant tubercle bacilli and latent tuberculosis. *Front Biosci* **9:** 1136–1156.